Journal of Fluorine Chemistry 272 (2023) 110191

Contents lists available at ScienceDirect

Journal of Fluorine Chemistry

journal homepage: www.elsevier.com/locate/fluor

The C—F···H—CF_2 interaction: A combination of hydrogen bonding and $n \rightarrow \sigma^*$ stabilization

Nathaniel G. Garrison [a], Stefan Andrew Harry [a], Maxime A. Siegler [a], Guilherme Cariello [b], Rodrigo A. Cormanich [b,*], Thomas Lectka [a,*]

[a] Department of Chemistry, Johns Hopkins University, 3400 North Charles St., Baltimore, MD 21218, United States
[b] Universidade Estadual de Campinas (UNICAMP), Instituto de Química, Departamento de Química Orgânica, Monteiro Lobato Street, Campinas, São Paulo, 13083-862, Brazil

ARTICLE INFO

Keywords:
Hydrogen bonding
Tetrel bonding
Difluoromethyl H-bonding
$n \rightarrow \sigma^*$ interaction

ABSTRACT

In this communication, we explore a unique molecule that exhibits a substantial interaction between a CF_2H group and a C—F group. In medicinal chemistry, CF_2H groups are known as weak hydrogen bond donors, and C—F groups as weak H-bond acceptors. Seldom are they paired up together in an array such that their unique properties can be examined. In this case, we establish that along with an attractive hydrogen bonding interaction, an $n \rightarrow \sigma^*$ component anchors the interactions. A unique combination of steric and hyperconjugative effects 'switches' the interaction away from previously reported dominant tetrel-type bonding in the case of a CH_2F and CF interation towards an unusualy complex hybrid interaction. Crystallographic, computational, and spectroscopic studies illuminate the problem.

1. Introduction

The —CF_2H group has attained a notable position in medicinal chemistry as a lipophilic surrogate for the acidic hydroxy group [1] that possesses the distinct ability to serve as a weak hydrogen bond donor [2]. This analogy is far from perfect – for example, unlike the oxygen atom, the carbon of the CF_2H group is electrophilic [3]. Still, for practical reasons the relationship often works. On the other hand, the C—F bond is recognized for its ability to serve as a hydrogen bond acceptor [4]; some of our prior work and studies from the labs of others have featured close interactions of hydroxy groups with C—F bonds that lead to fascinating hydrogen bonding arrays [5]. Imagine if you will the interaction between the CF_2H group and a C—F bond – what you would have is an unusual hydrogen bonding motif consisting solely of carbon, fluorine, and hydrogen. Interestingly enough, such interactions, albeit fairly weak, are replete within crystal structures of small molecules in the CSD (Fig. 1) [6]. The majority of the intermolecular arrays are bent, with a C—H—F bond angle averaging 130°, in stark contrast to stronger O—H—O hydrogen bonds in which the analogous arrays are typically (but not always) closer to linear [7].

In this note, we report a case of significant C—**F**···**H**—CF_2 hydrogen bonding in a rigid model system, and show how it compares and contrasts with the analogous C—**F**···**C**H_2F system that is noted for an n (C—F) $\rightarrow \sigma^*$ interaction [8]. This later mode has been described as a σ-hole or "tetrel" bond [9]. In a previous study on a C—**F**···**C**H_2F system, we provided direct experimental evidence for the significance of this interaction, concurring with prior computational and crystallographic studies.

Herein, we demonstrate that both systems represent an admixture of hydrogen bonding and n(C—F) $\rightarrow \sigma^*$ interactions, with *the balance moving towards hydrogen bonding* in the present system. This "switch," albeit subtle, sheds light on the nature of the delicate balance that can accompany hydrogen bonding interactions (Fig. 2).

2. Results and discussion

To begin our study, we elaborated a 4,5-disubstituted phenanthrene (candidate **2**, Fig. 3) [10] that holds the interacting hydrogen bond donor and acceptor in very close proximity [11]. Hexafluoride **2** can be made from the known dialdehyde **1** through high temperature DAST (diethylaminosulfurtrifluoride) treatment (Fig. 3) [12]. The ^{1}H NMR spectrum of **2** revealed some interesting features. For example, the probe CF_2H proton is almost 1 ppm downfield from that of the control; it also shows a large geminal J_{HF} coupling (66 Hz) but a much smaller

* Corresponding authors.
E-mail addresses: cormanich@unicamp.br (R.A. Cormanich), lectka@jhu.edu (T. Lectka).

https://doi.org/10.1016/j.jfluchem.2023.110191
Received 16 August 2023; Received in revised form 21 September 2023; Accepted 24 September 2023
Available online 26 September 2023

through-space coupling (3.7 Hz) to the aryl C—F. Perhaps most interesting is the $^{TS}J_{FC}$ "through-space" coupling of 30.4 Hz, an unusually large result for heavy atoms purported to engage in a hydrogen bonding array [13]. Most interestingly, this result implies the presence of an *n* (C—F) → *σ** contribution to the interaction. Coupling between C—**F**···C**F**$_2$H ($^{TS}J_{FF}$) is also substantial (13.2 Hz), further supporting *n* (C—F) → *σ** donation. The IR spectrum is somewhat difficult to interpret due to interfering C—H stretches. Still, a few general comments are in order. For example, DFT calculations (at M06/6–311+*G*** and other functionals) predict a typically energetic C—H stretch for the control C—H, and correspondingly strong red shifts for the probe C—H (69 cm^{-1} observed, 75 cm^{-1} calcd).

The crystal structure of **2** shows a C—**F**···**H**—CF$_2$ distance of 2.23(2) Å and a C—**F**···**C**F$_2$H distance of 2.5887(19) Å (Fig. 4). By comparing the crystal structures of **2** and tetrafluoride **3**, one can map the transformation from a predominately *n*(C—F) → *σ** interaction to a more significant hydrogen bonding array. For example, the C—**F**···**C**—F distance shortens in **3** (to 2.56 Å), whereas the C—**F**···**H**—CF distance lengthens (to 2.29 Å from 2.23 Å (M062X/6–311+*G*** C—**F**···**H**—CF$_2$ distance in **2** 2.21 Å; the original crystal structure was modified to reflect a more typical C—H DFT distance of 1.083 Å). The slightly lengthened interaction in the crystal probably reflects bifurcated H-bonding character between CF$_2$H groups in the packing.

To explore the interaction further, we employed a structured sequence of theoretical calculations and accessed accuracy with benchmarking experiments. We conducted a conformational analysis on a simplified version of molecule **2**, lacking the distal —F and —CF$_2$H, designated **2′** by using the recently developed CREST software of Grimme and coworkers [14]. A new geometry optimization was performed using a range of DFT functionals and basis sets that show a good correlation with experimental $^1J_{FC}$ values in a previous benchmarking study [15].

To evaluate the performance of different theoretical models, we computed spin-spin coupling constants (SSCCs) using 20 different theoretical levels in Gaussian 16 (see SI) [16]. The applied levels were divided into four groups based on their DFT functionals (B3LYP, BHandH, M06L, and PBE0) [17], and further subdivided into five basis sets (pc-0, pc-1, pc-2, EPR-III, and aug-cc-pVTZ for conformer reoptimization and pcJ-0, pcJ-1, pcJ-2, EPR-III, and aug-cc-pVTZ-J for SSCC calculations) [18]. After confirming the conformers were true minima with no negative frequencies, we compared the results to experimental J_{FH}, J_{FF} and J_{FC} SSCCs. This determined the accuracy of different theoretical models in predicting the conformer populations and SSCC values. This exhaustive benchmarking procedure is particularly important for SSCCs involving F atoms due to their unusually non-dominant Fermi contact (FC) interaction. Such behavior has stymied numerous attempted DFT investigations of fluorinated compounds and well-earning the moniker "the fluorine problem" [19].

With the best theoretical level in hand for each compound/SSCCs (Table 1), we ran NJC (natural J-coupling analysis) calculations to identify the transmission pathway of the SSCCs of interest. Natural J-coupling analysis allows for extracting information about the electronic

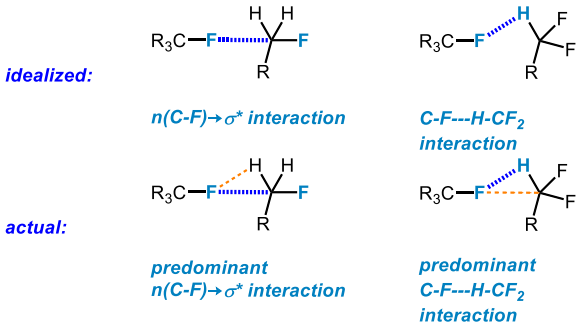

Fig. 2. Frozen C—F—C—X interactions.

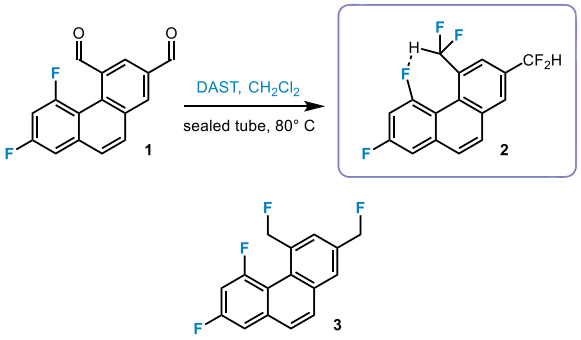

Fig. 3. Synthesis of **2**; compare to control **3.**

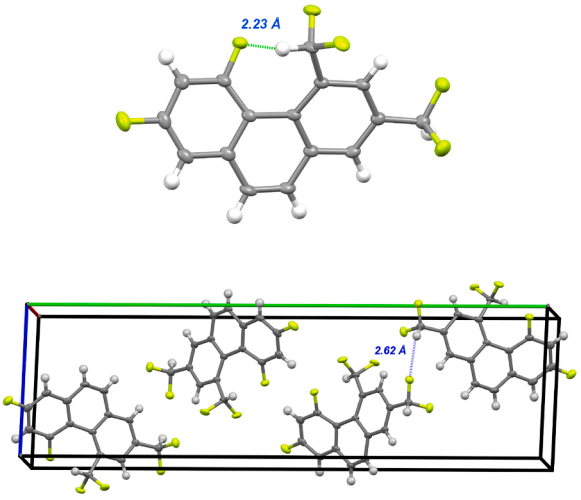

Fig. 4. Top: Crystal structure of **2**, 50 % thermal ellipsoids. Bottom: Packing diagram of **2**, showing close intermolecular C—F—H contacts.

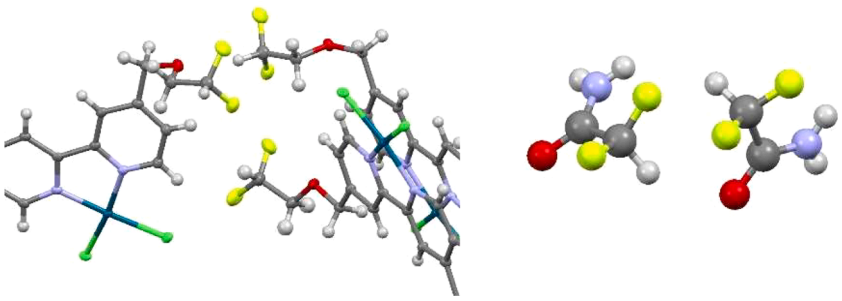

Fig. 1. Literature examples of CF$_2$H and C—F from the CSD. BEKBAX (left) [21] and DFACAM (right) [22].

Table 1
Benchmarking spin-spin coupling constants calculations for **2′** in $CHCl_3$. The values given were weighted-averaged over calculated conformer populations **2a′** and **2b′** in each level.

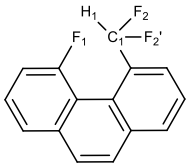

	JH1F1	JC1F1	JF1F2/JF1F2'
M06L/pcJ-0	−0.9	37.4	21.4
M06L/pcJ-1	12.3	32.9	20.1
M06L/pcJ-2	12.3	28.7	21.8
M06L/EPR-III	12.8	29.8	15.2
M06L/aug-cc-pVTZ-J	12.4	30.1	23.7
BHandH/pcJ-0	−3.7	53.6	35.8
BHandH/pcJ-1	8.6	47.6	20.1
BHandH/pcJ-2	9.3	42.8	19.2
BHandH/EPR-III	9.5	42.6	19.0
BHandH/aug-cc-pVTZ-J	9.5	43.4	19.7
Experimental	3.7	30.4	13.2

structure and bonding of molecules from their J-coupling constants. We have applied NJC analysis successfully in previous work to understand the SSCCs transmission pathway in conformers of fluorophenols and fluorothiophenols [20].

Three conformers (**2a'−2c'**) (Fig. 5) were found for **2′** across all theoretical levels. Interestingly, the pc-0 basis set indicates **2a'** as the most stable, accounting for ~99 % of the conformational population and presenting the best match with experimental J_{FH} SSCCs when tight *s*-basis functions are added (pcJ-0). Other basis sets indicate **2b'** as the most stable (this conformation maps well onto the crystal structure of **2**), with ~70 % of the conformer population, but show poor correlation with observed J_{FH} values (Table 1). However, the M06L functional combined with the EPR-III and aug-cc-pVTZ-J basis sets were the closest to experimental J_{FC} and J_{FF} SSCCs. This way, the high calculated population of **2a'** by the pc-0 basis set, together with a close calculated value of the J_{FH} SSCC to the experimental value explain its apparent accuracy. Furthermore, it is the only basis set that calculates a negative J_{FH} coupling constant (−3.7 Hz for BHandH/pcJ-0). This might be highly accurate based on the small experimental J_{FH} coupling constant of 3.7 Hz, but if the experimental SSCC sign is positive, it would diverge from the experimental value as much as the other basis sets. Among the tested functionals in this work, Gaussian 16 can calculate Grimme's D3 dispersion corrections for B3LYP, M06L and PBE0. The calculated Gibbs free energies/conformer populations do not show considerable change by including D3 dispersion corrections in B3LYP functional.

Therefrom, the calculated J_{FH} values were decomposed into FC, spin dipolar (SD), paramagnetic spin orbital (PSO), and diamagnetic spin orbital (DSO) Ramsey terms. The FC term is the most divergent between pc-0 (−2.61 Hz) and the other basis sets (ca. 9.0 Hz). Evidently the high percentage of conformer **2a'** calculated for BHandH/pc-0 and the negative FC term of BHandH/pcJ-0 are necessary to achieve good correlation with experimental J_{FH} values for **2**.

There is an important deviation from planarity for the anthracene rings in **2′**. The large steric clash between the F atom and CF_2H group results in a calculated (F)C—C—C—C(CF_2H) dihedral angle of ca. 20°, while crystallographic data from **2** indicates the dihedral angle is 26°. The anthracene ring deviates from planarity, decreasing the molecule's aromaticity and minimizing steric effects between the substituents. The equilibrium geometry of **2a'** shows a small C—**F**···**H**—CF_2 contact of 1.917 Å, indicating a strong non-conventional hydrogen bond (H-bond), presumably resulting in the high stability of this conformer. This relatively close contact in the context of the planar distortion and subsequent computational evidence effectively rule out a strictly steric explanation for the observed structure.

We surmised that this "switch" towards hydrogen bonding would be an ideal candidate for atoms-in-molecules (AIM) and NBO analyses. QTAIM shows a bond critical point (BCP) for the C—**F**···**H**—CF_2 hydrogen bond with an electron density (ρ) at BCP of $\rho = 0.034$ au and Laplacian of the electron density at BCP ($\nabla^2\rho$) of +0.164 au using M06/6–311+*G*** (Fig. 6), indicating a strong electrostatic character H-bond. This is supported by the NCI method and NBO analysis both as stereoelectronic [n(2)F12 → $\sigma^*_{C21–H25}$ = 2.71 kcal mol^{-1} hyperconjugation] and electrostatic in nature (−11.5 kcal mol^{-1} electrostatic stabilization energy when using NPA charges and the classic Coulomb equation). This result reenforces the concept that the observed stabilization cannot be entirely explained by the favorable alignment of CF and CF_2 dipoles.

The NJC analysis may decompose the FC term into its Lewis (steric) and non-Lewis (hyperconjugative) contributions (Table 2). NJC analysis indicates that the highest contribution to the observed $^1J_{FH}$ coupling constant is due to the stereoelectronic descriptor of the C—**F**···**H**—CF_2 H-bond (n(2)F12 → $\sigma^*_{C21–H25}$), which has a −33.35 Hz contribution to the Fermi Constant (FC) term. Such large contribution to the J_{FH} SSCC is largely attenuated by other stereoelectronic interactions (Fig. 7).

The evidence for hydrogen bond donating activity is further supported by a comparison to the previously published C—**F**—**C**H_2F system (**3**). But first, it is worth considering the limitations of a computational methodology optimized to match a J_{FH} coupling constant. QTAIM calculations exhibit a significant rotameric dependence and yield very different results when comparing BHandH/pcJ-0 to methods that adhere to the crystal structure more closely. Considering F_1—H_1 distance and the (F)C—C—C—C(CF_2H) dihedral angle, BHandH/pcJ-0 yields deviations of 0.32 Å and 5.69° while a methodology like M06–2X/6–311++*G*** differs by only 0.025 Å and 0.23° The latter method yields a C—**F**···**H**—CF_2 BCP of $\rho = 0.0177$ and similar results were replicated using B3LYP, ωB97XD and a BHandH run using the 6–311+*G*** basis set. In the M06-2X calculations, the bond critical point (BCP) between F and C seen in **3** disappears, to be replaced by the previously discussed F_1—H_1 BCP (Fig. 8). In any event, this suggests that the additional fluorine triggers a subtle transformation to hydrogen bond donor.

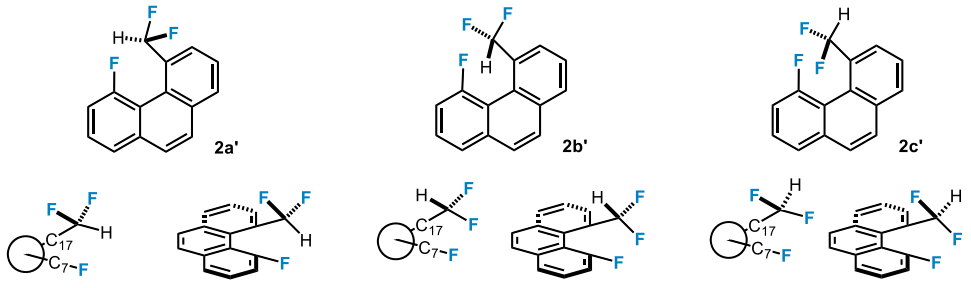

Fig. 5. Major calculated conformers with Newman projections oriented to the C_3–C_6 central bond of the (F)C—C—C—C(CF2H) dihedral angle with an additional structure depicting the orientation with regard to the twist in the phenanthrene core. The full carbon numbering scheme is depicted in Fig. 6.

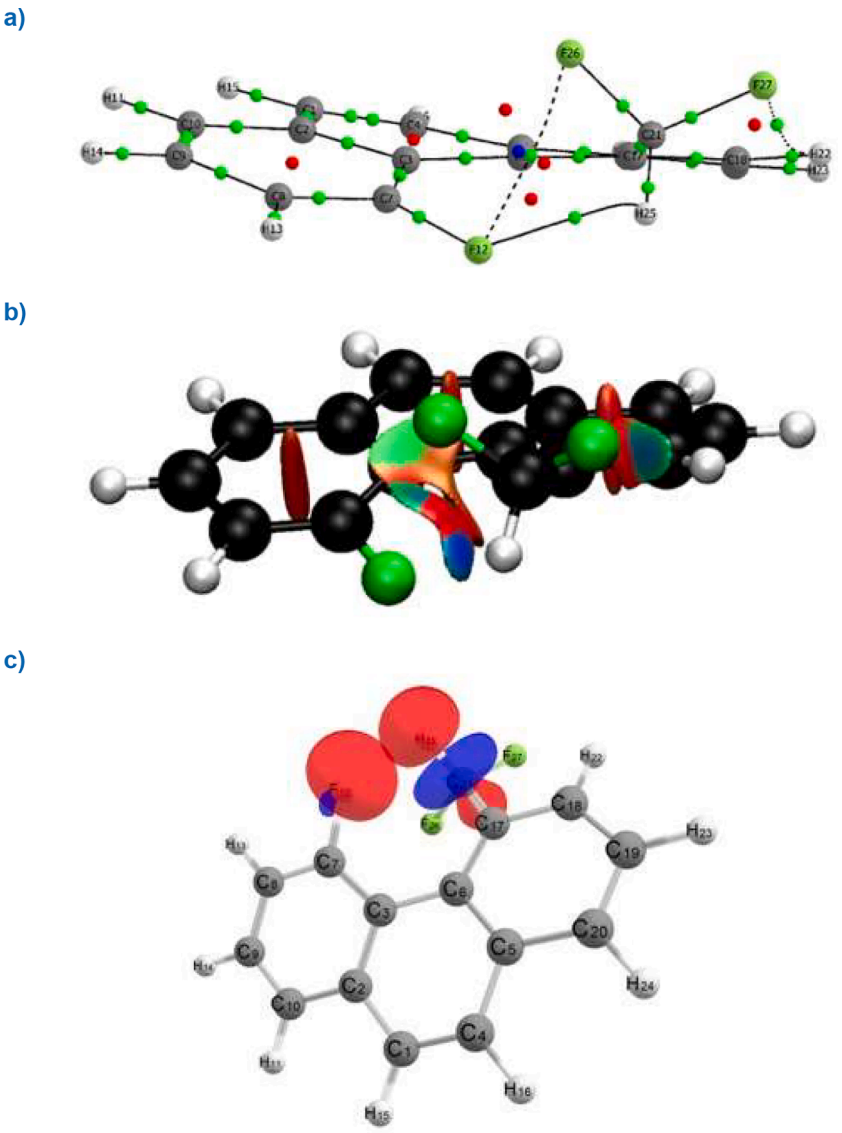

Fig. 6. a) QTAIM molecular graph: bond critical points (BCP, green), ring critical points (RCP, red) and cage critical point (CCP, blue). b) NCI isosurfaces using reduced density gradient (RDG) = 0.5 and blue-green-red color scale ranging from $-0.02 < \text{sign}(\lambda_2)\rho(r) < 0.02$ au. c) n(2)F12 → $\sigma^*_{C21-H25}$ hyperconjugative interaction obtained from the NBO analysis.(For interpretation of the references to color in this figure legend, the reader is referred to the web version of this article.)

Table 2
Natural J-coupling analysis at BHandH/pcJ-0 for the FC term of J_{FH} coupling constant of conformer **2a**′ in the gas phase. Main Lewis and delocalization contributions to the FC term are given in Hz.

J_{FH}	$J^{(FC)}$	$J^{(L)}$	$J^{(Repol)}$	$J^{(deloc)}$
−3.17	**−2.05**	**1.91**	**0.26**	**−4.21**

Intramolecular H-bond energies are generally arbitrary, but there is an equation developed within QTAIM where we can at least estimate the intramolecular H-bond energy at the BCP. For **2**, LP(F_a) → $\sigma^*C_aF_b$ is 4.48 kcal mol^{-1} (tetrel) and LP(F_a) → $\sigma^*C_aH_a$ is 3.24 kcal mol^{-1} (H-bonding). For **3**, LP(F_a) → $\sigma^*C_aF_b$ is 2.86 kcal mol^{-1} (tetrel) and LP(F_a) → $\sigma^*C_aH_a$ is 1.30 kcal mol^{-1} (H-bonding). Interestingly enough, both tetrel and H-bonding components are predicted to be enhanced in **2**(Fig. 9).

3. Conclusion

Our earlier work was consistent with an illustrative theoretical study that postulates the involvement of an n(C-F) → σ^* component of hydrogen bonding interactions in R_3C—H···X− arrays (X− = Cl−, Br−) [23]. In the present case, hydrogen bond donation plays a more prominent role. That both modes of interaction play a part, the significance of which can be influenced by nearby structural elements, further demonstrates the surprising complexity of hydrogen bonding interactions in general. Given the interest in the CF_2H group as a bioisostere in pharmacological contexts, understanding its unusual binding properties would be useful. For example, its hybrid tetrel/ hydrogen bonding interaction could prove important to targeting protein binding pockets or designing polymer morphologies. The ubiquity of hydrogen bonding interactions makes studying examples that deviate from conventional behavior even more valuable.

4. Experimental section

4.1. General information

Unless otherwise stated, all reactions were carried out under strictly anhydrous, air-free conditions under nitrogen. All solvents and reagents were dried and degassed by standard methods. ^{1}H and ^{13}C spectra were

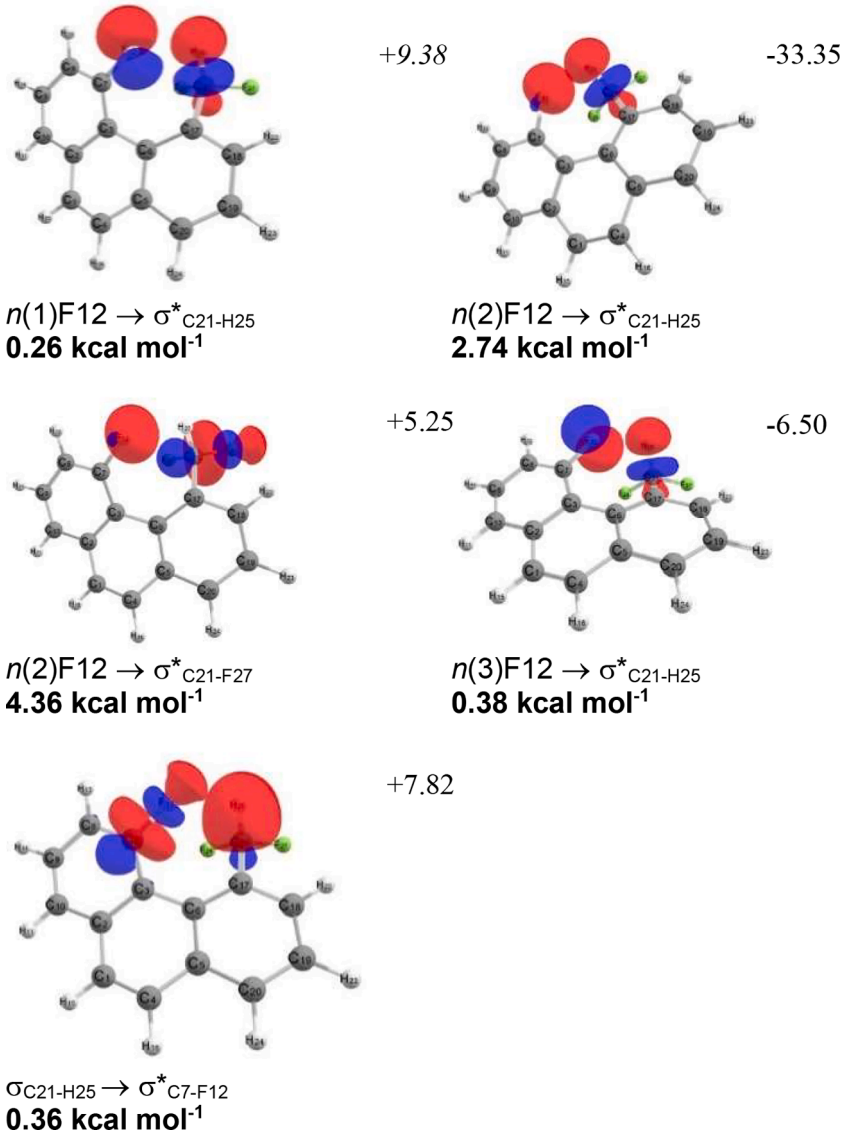

Fig. 7. The most important hyperconjugative Interactions for the total $J^{(deloc)}$ and hyperconjugative stabilization energy for each interaction (bold) for **2a**′ obtained from the NJC and NBO analysis.

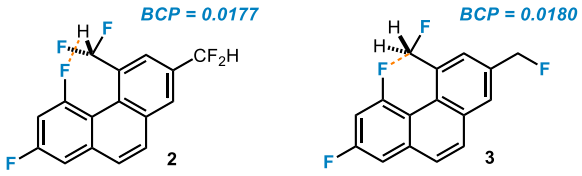

Fig. 8. Switch in bond critical points (BCPs) from **2** to **3**. Calculated using m062.

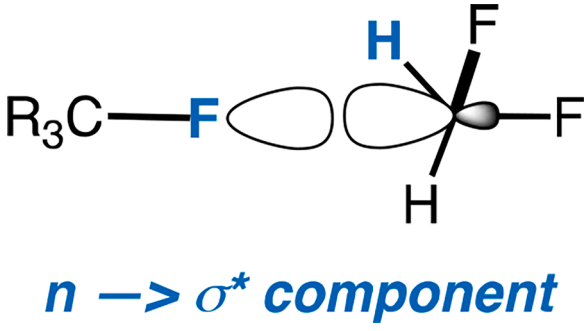

Fig. 9. A classical tetrel bonding interaction.

acquired on a 400 MHz NMR whereas ^{19}F NMR spectra were acquired on a 300 MHz NMR in $CDCl_3$ or CD_3CN at 25 °C (unless otherwise stated). The ^{1}H, ^{13}C and ^{19}F chemical shifts are given in parts per million (δ) with respect to an internal tetramethylsilane (TMS, δ 0.00 ppm) standard. NMR data are reported in the following format: chemical shifts (multiplicity (*s* = singlet, *d* = doublet, *t* = triplet, *q* = quartet *m* = multiplet), integration, coupling constants [Hz]). IR data were obtained using an FT-IR with a flat CaF_2 cell. HRMS data were obtained on a Thermo Scientific Q-Exactive Orbitrap mass spectrometer. All measurements were recorded at 25 °C unless otherwise stated. Spectral data were processed with ACD/NMR Processor Academic Edition. The Gaussian '09 package and Spartan '10 were used for all geometry optimizations [24,25]. All reflection intensities were measured at 110(2) K using a SuperNova diffractometer (equipped with Atlas detector) with Cu *Kα* radiation (*λ* = 1.54178 Å) under the program CrysAlisPro (Version 1.171.42.49, Rigaku OD, 2022). The same program was used to refine

the cell dimensions and for data reduction. The structure was solved with the program SHELXS-2018/3 (Sheldrick, 2018) and was refined on F^2 with SHELXL-2018/3 (Sheldrick, 2018). Analytical numeric absorption correction using a multifaceted crystal model using CrysAlisPro. The temperature of the data collection was controlled using the system Cryojet (manufactured by Oxford Instruments). The H atoms were placed at calculated positions (unless otherwise specified) using the instructions AFIX 43 with isotropic displacement parameters having values 1.2 U_{eq} of the attached C atoms. The H atoms attached to C15 and C16 were found from difference Fourier maps, and their coordinates were refined pseudofreely using the DFIX instruction so that the C—H bond distances match those determined from DFT calculations. The structure is ordered.

4.2. Experimental procedures

5,7-difluorophenanthrene-2,4-dicarbaldehyde (1): 2,4-bis(bromomethyl)-5,7-difluorophenanthrene (500 mg, 1.25 mmol) was dissolved in 40 mL acetonitrile containing silver nitrate (1.1 g, 6.25 mmol) at room temperature and then the mixture was refluxed for 2 h. After the ^{1}H NMR of the mixture revealed complete conversion of the starting material, it was filtered over celite, and the solvent was evaporated under reduced pressure. The intermediate nitrate ester was dissolved in 50 mL ethanol, Pd/C (50 mg) was added, and the mixture was treated with hydrogen gas until ^{1}H NMR revealed complete conversion to the intermediate dialcohol. After filtering out excess Pd/C and evaporation of the solvent, the mixture was dissolved in 40 mL anhydrous dichloromethane. To the mixture were added molecular sieves (2 g), potassium carbonate (1.2 g, 8.7 mmol) and PCC (590 mg, 2.75 mmol) and stirred at room temperature for 2 h. Upon completion, the mixture was filtered over celite, and solvent was evaporated under reduced pressure. The final product was isolated with silica gel chromatography using 10 % ethyl acetate in hexanes as a light-yellow solid (277 mg, 82 % yield). ^{1}H NMR (400 MHz, $CDCl_3$) δ 10.24–10.29 (d, J = 14 Hz, 1H), 10.27 (s, 1H), 8.49–8.63 (m, 2H), 7.88–7.96 (m, 1H), 7.78–7.86 (m, 1H), 7.45–7.53 (m, 1H), 7.15–7.24 (m, 1H); ^{13}C{H} NMR (101 MHz, $CDCl_3$) δ 190.8, 189.2 (d, 15.6 Hz), 163.4 (m), 161.5 (m), 160.9 (m), 158.9 (m), 137.0 (m), 135.5 (m), 134.3, 134.1, 132.7 (m), 129.1 (m), 128.3, 127.9 (m), 114.4 (m), 109.4 (m), 104.2, 103. 9 (m), 103.6; ^{19}F NMR (282 MHz, $CDCl_3$) δ –105.3 (1F, m), –106.2 (1F, m); FTMS + p (ESI) calc for $C_{16}H_9O_2F_2^+$: 271.0571, found 271.0568.

2,4-bis(fluoromethyl)-5,7-difluorophenanthrene (3): Compound **3** was synthesized following previously reported protocols [10]. Yield 98 %. White solid. FTIR (neat) cm^{-1}: 3079.46, 2969.49, 2923.92, 2895.65, 2852.97, 1649.86, 1380.97, 1311.72; ^{1}H NMR (400 MHz, $CDCl_3$) δ 5.63 (d, J = 47.44 Hz, 2 H) 5.80 (dd, J = 48.32, 7.14 Hz, 2 H) 7.11 (ddd, J = 12.59, 8.39, 2.59 Hz, 1 H) 7.40 (dd, J = 8.56, 1.61 Hz, 1 H) 7.62 (dd, J = 8.80, 1.86 Hz, 1 H) 7.73 (d, J = 8.80 Hz, 1 H) 7.87 (d, J = 10.56 Hz, 2 H); ^{13}C{H} NMR (101 MHz, $CDCl_3$) δ 83.02 (dd, J = 163.96, 41.45 Hz) 83.98 (d, J = 167.63 Hz) 102.59 (t, J = 28.20 Hz) 108.46–108.97 (m) 114.79 (d, J = 16.51 Hz) 124.55 (br. s.) 125.75 - 126.06 (m) 126.45 (dd, J = 6.79, 2.38 Hz) 129.43 (s) 132.26 (s) 134.91 (d, J = 17.60 Hz) 135.39 (d, J = 16.51 Hz) 136.00 (dd, J = 10.09, 6.05 Hz) 158.09 (d, J = 12.47 Hz) 159.66 (d, J = 13.94 Hz) 160.60 (d, J = 12.47 Hz) 162.14 (d, J = 13.94 Hz); ^{19}F NMR ($CDCl_3$) δ −209.26 (t, J = 47.60 Hz, 1 F) −198.68 (td, J = 48.20, 6.32 Hz, 1 F) −110.46 (q, J = 8.61 Hz, 1 F) −106.40 - −106.19 (m, 1 F). TOF MS (FD+) calc for $C_{16}H_{10}F_4^+$: 279.07914, found: 279.09250. While this result is outside the typically accepted 0.003 m/z range, we believe successful characterization by X-ray crystallography adequately supports our proposed structure.

2,4-bis(difluoromethyl)-5,7-difluorophenanthrene (2): The dialdehyde **1** (15 mg, 0.056 mmol) was dissolved in dichloromethane (3 mL) inside a Schlenk tube, excess diethylaminosulfur trifluoride (0.2 mL 1.51 mmol) was added dropwise at room temperature under N_2. The tube was sealed, heated to 80 °C and left stirring overnight. After aliquot was taken and the ^{19}F NMR confirmed reaction completion, the mixture was cooled to room temperature and diluted with 10 mL of dichloromethane before being quenched with 20 mL water. The mixture was then extracted with 10 mL dichloromethane three times, dried over anhydrous sodium sulfate, and the organic solvents were evaporated under reduced pressure. The doubly difluoronated **2** was isolated with silica gel chromatography using 25 % ethyl acetate in hexanes as a white solid (13.4 mg 76 %); FTIR (neat) cm^{-1}: 2952.65, 2921.79, 2852.90, 1630.14, 1580.99, 1455.80, 1376.66, 1128.28, 1069.94; ^{1}H NMR (400 MHz, $CDCl_3$) δ 8.13 (d, J = 5.6 Hz, 2H), 7.79 (d, J = 8.9 Hz, 1H), 7.71 (dd, J = 8.8, 1.7 Hz, 1H), 7.36 (td, J = 55.7, 3.7 Hz, 3H), 6.93 (t, J = 55.9 Hz, 1H); ^{13}C{H} NMR (101 MHz, $CDCl_3$) δ 162.66 (d, J = 13.9 Hz), 160.87 (d, J = 12.1 Hz), 160.16 (d, J = 13.9 Hz), 158.37 (d, J = 13.2 Hz), 136.33 (dd, J = 10.3, 5.5 Hz), 133.78 (t, J = 22.4 Hz), 132.69 (m), 129.03 (s), 127.63 (t, J = 6.4 Hz), 127.05 (t, J = 3.3 Hz), 125.30 (s), 123.55 (t, J = 7.0 Hz), 116.11 (m), 114.47 (s), 113.73 (m), 111.36 (m), 113.60 (td, J = 236.2, 30.4 Hz), 113.96 (t, J = 239.5 Hz), 108.95 (m), 103.13 (m); ^{19}F NMR (282 MHz, $CDCl_3$) δ −104.47 (m), −106.50 (dd, J = 55.6, 13.2 Hz), −108.85 (dd, J = 18.4, 8.6 Hz), −111.05 (d, J = 56.2 Hz); HRMS (TOF-FD+) m/z $[M^\bullet]^+$ calc for $C_{16}H_8F_6^+$: 314.0557, found: 314.0530. The X ray-crystallography sample was prepared by slow evaporation from a 50:50 solution of ethyl acetate and methanol.

Declaration of Competing Interest

The authors declare no competing financial interest.

Data availability

Data will be made available on request.

Acknowledgment

T.L. thanks the National Science Foundation (NSF) (Grant no. CHE 2102116) for financial support. R.A.C. thanks FAPESP (#2018/03910-1) for a Young Researcher Award and CNPq for a scholarship (G.C.). CENAPAD-SP, CESUP and SDumont are also acknowledged for the computational resources used in theory calculations. Mass spectral data were obtained at University of Delaware's mass spectrometry centers.

Supplementary materials

Supplementary material associated with this article can be found, in the online version, at doi:10.1016/j.jfluchem.2023.110191.

References

[1] a) M.G. Blackburn, D.E. Kent, F. Kolkmann, Three new β,γ-methylene analogues of adenosine triphosphate, J. Chem. Soc., Chem. Commun. 22 (1981) 1188–1190; b) S. Saphier, S. Katalan, G. Yacov, A. Berliner, O. Redy-Keisar, G. Fridkin, L. Ghindes-Azaria, I. Columbus, A. Pevzner, E. Drug, H. Prihed, E. Gershonov, Y. Eichen, S. Elias, G. Parvari, Y. Zafrani, Placing CF_2 in the center: major physicochemical changes upon a minor structural alteration in gem-difunctional compounds, Chem. Eur. J. 29 (2023), e202202939.

[2] Y. Zafrani, G. Sod-Moriah, D. Yeffet, A. Berliner, D. Amir, D. Marciano, S. Elias, S. Katalan, N. Ashkenazi, M. Madmon, E. Gershonov, S. Saphier, CF2H, a functional group-dependent hydrogen-bond donor: is it a more or less lipophilic bioisostere of OH, SH, and CH_3? J. Med. Chem. 62 (2019) 5628–5637.

[3] S. Scheiner, Systematic elucidation of factors that influence the strength of tetrel bonds, J. Phys. Chem. A 121 (29) (2017) 5561–5568.

[4] C. Dalvit, C. Invernizzi, A. Vulpetti, Fluorine as a hydrogen-bond acceptor: experimental evidence and computational calculations, Chem. Eur. J. 20 (2014) 11058–11068.

[5] M.G. Holl, C.R. Pitts, T. Lectka, Fluorine in a C–F bond as the key to cage formation, Angew. Chem. Int. Ed. 57 (2018) 2758–2766.

[6] H.J. Schneider, Hydrogen bonds with fluorine. Studies in solution, in gas phase and by computations, conflicting conclusions from crystallographic analyses, Chem. Sci. 3 (2012) 1381–1394.

[7] a) J.D. Dunitz, T. Robin, Organic fluorine hardly ever accepts hydrogen bonds, Eur. J. Chem. 3 (1997) 89–98;

b) A. Daolio, P. Scilabra, G. Terraneo, G. Resnati, C(sp3) atoms as tetrel bond donors: a crystallographic survey, Coord. Chem. Rev. 413 (2020), 213265.

[8] S.A. Harry, N.G. Garrison, A. Zhu, M.R. Xiang, M.A. Siegler, T. Lectka, C–F bonds as "frozen" nucleophiles: unconsummated S_N2 reactions, J. Org. Chem. 87 (19) (2022) 13406–13410.

[9] a) A. Bundhun, P. Ramasami, J.S. Murray, P. Politzer, Trends in σ-hole strengths and interactions of F3MX molecules (M = C, Si, Ge and X = F, Cl, Br, I), J. Mol. Model. 19 (2013) 2739–2746;
b) A. Bauzá, T.J. Mooibroek, A. Frontera, Tetrel-bonding interaction: rediscovered supramolecular force? Angew. Chem. Int. Ed. 52 (2013) 12317–12321;
c) D. Mani, E. Arunan, The X–C···Y (X = O/F, Y = O/S/F/Cl/Br/N/P) 'carbon bond' and hydrophobic interactions, Phys. Chem. Chem. Phys. 15 (2013) 14377–14383.

[10] a) R. Cosmo, T.W. Hambley, S. Sternhell, Skeletal deformation in 4,5-disubstituted 9,10-dihydrophenanthrenes and 4,5-disubstituted phenanthrenes, J. Org. Chem. 52 (1987) 3119–3123;
b) R. Cosmo, S. Sternhell, Steric effects. Inversion of 4,5-disubstituted 9,10-dihydrophenanthrenes, Aus. J. Chem 40 (1987) 35–47;
c) M.S. Newman, W.B. Wheatley, Optical activity of the 4, 5-phenanthrene type: 4-(1-methylbenzo[*c*]phenanthryl)-acetic acid and 1-methylbenzo[*c*]phenanthrene, J. Am. Chem. Soc. 70 (1948) 1913–1916.

[11] We recently used this scaffold to examine the close interaction of a C–F bond with an amide carbonyl group S.A. Harry, M. Kazim, P.M. Nguyen, A. Zhu, M.R. Xiang, J. Catazaro, M. Siegler, T. Lectka, The close interaction of a C–F bond with an amide carbonyl: crystallographic and spectroscopic characterization, Angew. Chem. Int. Ed. 61 (2022), e202207966.

[12] R. Szpera, D.F.J. Moseley, L.B. Smith, A.J. Sterling, V. Gouverneur, The fluorination of C−H bonds: developments and perspectives, Angew. Chem. Int. Ed. 58 (2019) 14824–14848.

[13] M. Jaszuński, P. Świder, S.P.A. Sauer, Through-space spin–spin coupling constants involving fluorine: benchmarking DFT functionals, Mol. Phys. 117 (2019) 1469–1480.

[14] P. Pracht, F. Bohle, S. Grimme, Automated exploration of the low-energy chemical space with fast quantum chemical methods, Phys. Chem. Chem. Phys. 22 (2020) 7169–7192.

[15] M. De. Giovanetti, L. Felipe, F. Bitencourt, R. Cormanich, S.P.A. Sauer, On the unexpected accuracy of the M06L functional in the calculation of $^1J_{FC}$ spin–spin coupling constants, J. Chem. Theory Comput. 17 (2021) 7712–7723.

[16] M.J. Frisch, G.W. Trucks, H.B. Schlegel, G.E. Scuseria, M.A. Robb, J.R. Cheeseman, G. Scalmani, V. Barone, G.A. Petersson, H. Nakatsuji, et al., Gaussian 16, Revision C.01, Gaussian 16, revision C.01; Gaussian, Inc.: Wallingford, CT, 2016. M.J. Frisch, G.W. Trucks, H.B. Schlegel, G.E. Scuseria, M.A. Robb, J.R. Cheeseman, G. Scalmani, V. Barone, G. A. Petersson, H. Nakatsuji, X. Li, M. Caricato, A. V. Marenich, J. Bloino, B. G. Janesko, R. Gomperts, B. Mennucci, H. P. Hratchian, J. V. Ortiz, A. F. Izmaylov, J. L. Sonnenberg, D. Williams-Young, F. Ding, F. Lipparini, F. Egidi, J. Goings, B. Peng, A. Petrone, T. Henderson, D. Ranasinghe, V. G. Zakrzewski, J. Gao, N. Rega, G. Zheng, W. Liang, M. Hada, M. Ehara, K. Toyota, R. Fukuda, J. Hasegawa, M. Ishida, T. Nakajima, Y. Honda, O. Kitao, H. Nakai, T. Vreven, K. Throssell, J. A. Jr. Montgomery, J. E. Peralta, F. Ogliaro, M. J. Bearpark, J. J. Heyd, E. N. Brothers, K. N. Kudin, V. N. Staroverov, T. A. Keith, R. Kobayashi, J. Normand, K. Raghavachari, A. P. Rendell, J. C. Burant, S. S. Iyengar, J. Tomasi, M. Cossi, J. M. Millam, M. Klene, C. R. Adamo, R. Cammi, J. W. Ochterski, R. L. Martin, K. Morokuma, O. Farkas, J. B. Foresman, D.J. Fox, Gaussian, Inc., Wallingford, CT, 2016.

[17] a) J. Tirado-Rives, W.L. Jorgensen, Performance of B3LYP density functional methods for a large set of organic molecules, J. Chem. Theory Comput. 4 (2008) 297–306;
b) Y. Zhao, D.G. Truhlar, The M06 suite of density functionals for main group thermochemistry, thermochemical kinetics, noncovalent interactions, excited states, and transition elements: two new functionals and systematic testing of four M06-class functionals and 12 other functionals, Theor. Chem. Acc. 120 (2008) 215–241.

[18] a) C. Adamo, V. Barone, Toward reliable density functional methods without adjustable parameters: the PBE0 model, J. Chem. Phys. 110 (1999) 6158–6170;
b) B.P. Pritchard, D. Altarawy, B. Didier, T.D. Gibson, T.L. Windus, A new basis set exchange: an open, up-to-date resource for the molecular sciences community, J. Chem. Inf. Model. 59 (2019) 4814–4820.

[19] a) V.G. Malkin, O.L. Malkina, D.R. Salahub, Calculation of spin-spin coupling constants using density functional theory, Chem. Phys. Lett. 221 (1994) 91–99;
b) O.L. Malkina, D.R. Salahub, V.G. Malkin, Nuclear magnetic resonance spin-spin coupling constants from density functional theory: problems and results, J. Chem. Phys. 105 (1996) 8793–8800;
c) T. Helgaker, M. Watson, N.C. Handy, Analytical calculation of nuclear magnetic resonance indirect spin-spin coupling constants at the generalized gradient approximation and hybrid levels of density functional theory, J. Chem. Phys. 113 (2000) 9402–9409;
d) V. Sychrovsky, J. Gräfenstein, D. Cremer, Nuclear magnetic resonance spin-spin coupling constants from coupled perturbed density functional theory, J. Chem. Phys. 113 (2000) 3530–3547;
e) P. Lantto, J. Vaara, T. Helgaker, Spin-spin coupling tensors by density-functional linear response theory, J. Chem. Phys. 117 (2002) 5998–6009;
f) V. Barone, P.F. Provasi, J.E. Peralta, J.P. Snyder, S.P.A. Sauer, R.H. Contreras, Substituent effects on scalar $^2J(^{19}F,^{19}F)$ and $^3J(^{19}F,^{19}F)$ NMR couplings: a comparison of SOPPA and DFT methods, J. Phys. Chem. A. 107 (2003) 4748–4754.

[20] a) V.C. Port, L.A. Zeoly, F. Coelho, R.A. Cormanich, Through space J_{FH} spin–spin coupling constant transmission pathways in 2-(trifluoromethyl)thiophenol: formation of unusual stabilizing bifurcated CF···HS and CF···SH interactions, Phys. Chem. Chem. Phys. 23 (2021) 9080–9088;
b) L.A. Zeoly, F. Coelho, R.A. Cormanich, Intramolecular H-bond is formed in 2-fluorophenol and 2-fluorothiophenol, but it may not be the main pathway of the JFH coupling constant transmission, J. Phys. Chem. A. 123 (46) (2019) 10072–10078.

[21] N. Lu, J.-H. Zheng, Y.-J. Lu, H.-F. Chiang, C.-W. Chu, J.S. Thrasher, Y.-S. Wen, L.-K. Liu, Side-chain conformations in the isomorphous polyfluorinated {4,4′-*bis*[(2,2-difluoroethoxy)methyl]-2,2′-bipyridine-κ2*N*,*N*′}dichloridopalladium and -platinum complexes, Acta Cryst. C73 (2017) 930–936.

[22] D.O. Hughes, R.W.H. Small, The crystal and molecular structure of difluoroacetamide, Acta Cryst. B28 (1972) 2520–2524.

[23] A.Y. Li, Chemical origin of blue- and redshifted hydrogen bonds: intramolecular hyperconjugation and its coupling with intermolecular hyperconjugation, J. Chem. Phys. 126 (2007), 154102.

[24] M.J. Frisch, et al., Gaussian 09, Revision A.1, Gaussian, Inc., Wallingford CT, 2009.

[25] Spartan '10 Program, Wavefunction Inc., Irvine, CA.